RESEARCH ARTICLE | OCTOBER 04 2013

Effect of Mn doping on the structural, optical, and magnetic properties of In$_2$O$_3$ films ⊘

Shiqi Wang; Yukai An; Lingshen Duan; Huarui Liu; Jiwen Liu; Zhonghua Wu

Check for updates

View Online

Export Citation

Effect of Mn doping on the structural, optical, and magnetic properties of In$_2$O$_3$ films

Shiqi Wang, Yukai An,[a)] Lingshen Duan, Huarui Liu, and Jiwen Liu
Key Laboratory of Display Materials and Photoelectric Devices, Ministry of Education; Tianjin Key Laboratory for Photoelectric Materials and Devices; and School of Material Science and Engineering, Tianjin University of Technology, Tianjin 300384, China

Zhonghua Wu
Beijing Synchrotron Radiation Facility (BSRF), Institute of High Energy Physics, Chinese Academy of Sciences, Beijing 100049, China

($In_{1-x}Mn_x$)$_2$O$_3$ films were grown by radio frequency-magnetron sputtering technique. Effect of Mn doping on the structural, optical, and magnetic properties of films is investigated systematically. The detailed structure analyses suggest that Mn ions substitute for In^{3+} sites of the In$_2$O$_3$ lattice in the valence of +2 states, and Mn-related secondary phases or clusters as the source of ferromagnetism is safely ruled out. All films show typical room temperature ferromagnetism. The saturation magnetization M_s increases first, and then decreases, while carrier concentration n_c decreases monotonically with Mn doping, implying that the ferromagnetism is not directly induced by the mediated carriers. The optical bandgap E_g of films decreases monotonically with the increase of Mn concentration, and there exists a linear functional dependence between E_g and $n_c^{2/3}$, which is consistent with Burstein-Moss shift arguments. It can be concluded that the ferromagnetic order in Mn-doped In$_2$O$_3$ films is intrinsic, arising from Mn atoms substitution for the In sites of In$_2$O$_3$ lattice. The oxygen vacancies play a mediation role on the ferromagnetic couplings between the Mn ions. © *2013 American Vacuum Society.* [http://dx.doi.org/10.1116/1.4824163]

I. INTRODUCTION

Diluted magnetic semiconductors (DMSs), in which the cations are partially replaced by the transition metal (TM) in host lattice sites, have attracted a great deal of interest due to their potential applications in spintronic devices.[1] Since theoretical calculations on the basis of Zener's p-d exchange model predicted that room temperature (RT) DMSs may be realized in wide-band-gap semiconductors, a variety of TM-doped oxides, such as ZnO,[2,3] SnO$_2$,[4] TiO$_2$,[5] and In$_2$O$_3$,[6] were investigated extensively. Among these hosts, In$_2$O$_3$ is a technologically important n-type wide band-gap (3.75 eV) semiconductor with high electronic carrier concentration and mobility, and has been widely used as the transparent electrode by alloying with Sn. Recently, much attention has been paid to potential DMS behaviors of In$_2$O$_3$; RT ferromagnetism has been observed in a series of doped In$_2$O$_3$ films, such as Mn:In$_2$O$_3$,[7] Co:In$_2$O$_3$,[8,9] Fe:In$_2$O$_3$,[10,11] Cr:In$_2$O$_3$,[12,13] Ni:In$_2$O$_3$,[14,15] and Mo:In$_2$O$_3$.[16,17] However, the origin of ferromagnetism in this system still remains controversial; numerous results attributed the observed ferromagnetism to the intrinsic DMS property,[10] carrier-mediated,[17,18] defects-related effects,[9,14,19] and the formation of secondary phases.[20] Therefore, in order to gain insight into the origin of ferromagnetism in In$_2$O$_3$-based DMS, the further experimental investigations between the local structure and ferromagnetism are of great importance. In this paper, the effect of Mn doping on the structural, optical, and magnetic properties of films is discussed in great detail. The x-ray absorption spectroscopy (XAS) is employed for the study of local

atomic structure of Mn atoms inside the In$_2$O$_3$ lattice. The XAS measurements are correlated with structural investigations by UV-vis transmission spectra as well as magnetic and transport properties of films, which will be useful in advancing the studies on diluted magnetic semiconductors. These results can lay a strong foundation for discussing the origin and mechanism of ferromagnetism in Mn-doped In$_2$O$_3$ system.

II. EXPERIMENT

($In_{1-x}Mn_x$)$_2$O$_3$ films with a thickness of 900 nm were deposited on (*001*)Si and ultrawhite glass substrates by RF-magnetron sputtering. The sputter chamber was evacuated to a pressure less than 8×10^{-5} Pa before the deposition. The films were sputtered in 0.8 Pa of pure argon at a substrate temperature of 400 °C. To change the concentration of oxygen vacancy, the argon flow rate is fixed at 10 sccm, and the oxygen flow rate is varied from 0 sccm to 1.8 sccm. An In$_2$O$_3$ target (99.995%) with some Mn chips (99.995%) symmetrically attached was used to deposit Mn-doped In$_2$O$_3$ films. By adjusting the number of Mn chips, the ($In_{1-x}Mn_x$)$_2$O$_3$ films with x = 0.04, 0.05, 0.085, and 0.137 were readily fabricated. The Mn concentration in the films was determined by the x-ray energy dispersive spectroscopy (EDS). The crystal structures of films were examined by $\theta/2\theta$ x-ray diffraction (XRD) with Cu K$_\alpha$ radiation ($\lambda = 0.15406$ nm). The optical transmittance and absorption coefficient measurements were carried out using TU-1901 UV-visible spectrophotometer with scanning wavelength from 190 to 800 nm. The Mn K-edge x-ray absorption spectra (XAS) were measured by the total fluorescence mode at

a)Electronic mail: ayk_bj@126.com

Beijing Synchrotron Radiation on the 4B9A beamline of x-ray diffraction station. The Mn K-edge XAS measurements were obtained in two energy regions: x-ray absorption near-edge structure (XANES) and extend x-ray absorption fine structure (EXAFS). Hall effect measurements were made using the van der Pauw four-probe configuration with a magnetic field of 6 kOe. The magnetic properties measurements were performed as a function of magnetic field (0 to ± 15 kOe) using the physical properties measurement system (PPMS-9 Quantum Design) at room temperature.

III. RESULTS AND DISCUSSION

Figure 1 shows the θ–2θ XRD patterns of the $(In_{1-x}Mn_x)_2O_3$ (x = 0, 0.04, 0.05, 0.085, and 0.137) films. It is clear that all peaks displayed on the diffractogram could be indexed as In_2O_3 bixbyite cubic structure with a preferred (222) orientation. No detectable peaks corresponding to any Mn metal clusters or Mn oxide secondary phases were found with the XRD detection limit. A clear shift in the In_2O_3 (222) diffraction peaks to higher 2θ angles with the increase of Mn concentration is observed and suggests a gradual decrease in the average lattice parameter a (shown in the inset of Fig. 1). This is evidence that the smaller Mn ions (Mn^{2+} and Mn^{3+} ionic radius are 0.83 and 0.64 Å, respectively, compared to 0.94 Å for In^{3+}) are incorporated into In sites of the In_2O_3 lattice.[21,22] However, since the XRD method is not sensitive enough to detected nanoscale precipitates, we cannot exclude the existence of magnetic impurity phases; further characterization is necessary to obtain the detailed structure information.

The XANES/EXAFS techniques have been established as a powerful method to understand the local structure of TM-doped oxide systems. XANES is a fingerprint of the valence state and neighbor environment of TM cations in the host matrix and is highly sensitive to the precipitation of metal clusters or secondary magnetic phases, whereas the quantitative structural information about the metal environment can be obtained from the EXAFS analysis. The Mn K-edge XANES spectra of the $(In_{1-x}Mn_x)_2O_3$ (x = 0.04, 0.05, 0.085,
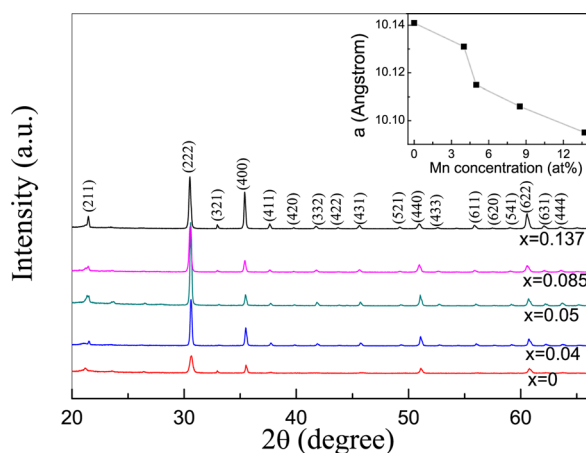
FIG. 2. (Color online) Mn K-edge XANES spectra of the $(In_{1-x}Mn_x)_2O_3$ (x = 0.04, 0.05, 0.085, and 0.137) films as well as Mn, MnO, and Mn_2O_3 foil.

and 0.137) films are shown in Fig. 2. As a guide to the valence state of Mn ions, reference Mn K-edge XANES spectra of standard Mn metal and Mn oxide (MnO and Mn_2O_3) are also displayed. The XANES spectral features of films are obviously different from those of standard Mn metal and of MnO or Mn_2O_3, indicating that the surrounding environment of the doped Mn atoms is rather different from those of standard Mn metal and Mn oxides. So the existence of Mn metal and Mn oxide in films can be safely excluded. It is clear that the absorption edge position of the films has close proximity to that of MnO reference, in marked contrast with those characteristics of Mn metal and Mn_2O_3, revealing that the Mn ions are in the +2 state. In addition, a clear 1s-3d pre-edge absorption peak around 6.538 keV (marked by an arrow in Fig. 2), typical of Mn ions in octahedral coordination of oxygen atoms, is also observed.

Figure 3 shows Fourier transform (FT) curves of Mn K-edge EXAFS oscillation functions $k^3\chi(k)$ for the

FIG. 1. (Color online) θ–2θ XRD patterns of the $(In_{1-x}Mn_x)_2O_3$ (x = 0, 0.04, 0.05, 0.085, and 0.137) films. The inset shows the decrease in the average lattice parameter, a (Å), as a function of Mn concentration.
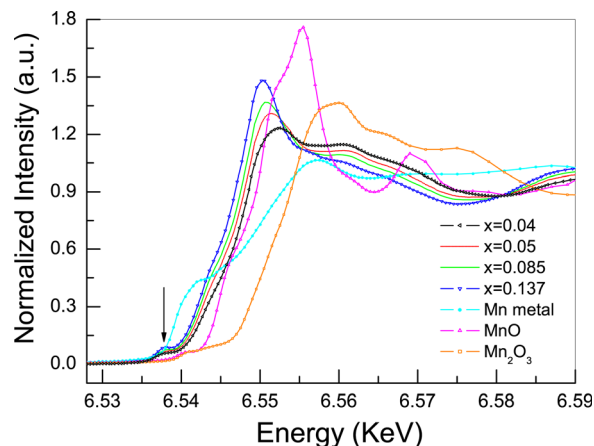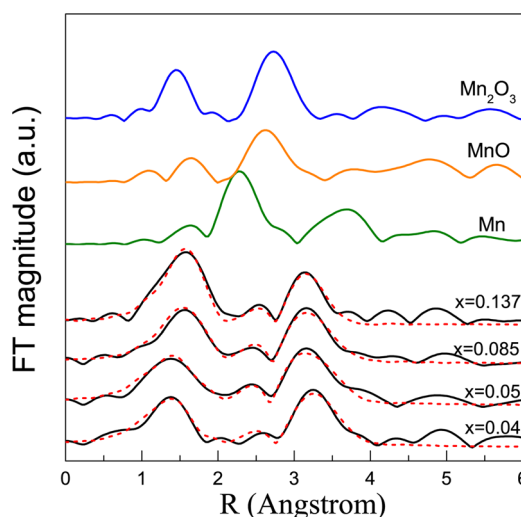
FIG. 3. (Color online) Experimental and fitting Fourier transform curves of Mn K-edge EXAFS oscillation functions $k^3\chi(k)$ for the $(In_{1-x}Mn_x)_2O_3$ (x = 0.04, 0.05, 0.085, and 0.137) films as well as Mn, MnO, and Mn_2O_3 foil. Solid lines: experimental; dashed lines: fitting for the $(In_{1-x}Mn_x)_2O_3$ (x = 0.04, 0.05, 0.085, and 0.137) films.

$(In_{1-x}Mn_x)_2O_3$ (x = 0.04, 0.05, 0.085, and 0.137) films as well as standard Mn metal and Mn oxide (MnO and Mn_2O_3). One can see that three peaks can be clearly observed at longer radial distance, suggesting that the local structure around Mn atoms is rather ordered with respect to short range ordering for the films. For the $(In_{1-x}Mn_x)_2O_3$ films with x = 0.04, 0.05, the three peaks at around 1.38, 2.48, and 3.23 Å are corresponding to the first Mn-O, the second Mn-In and the third Mn-In nearest neighbor coordination shell. The position of these peaks is obviously different from Mn metal (2.26 and 3.69 Å), MnO (1.64 and 2.62 Å), and Mn_2O_3 (1.45 and 2.72 Å). These further confirm that Mn ions substitute for the In^{3+} sites of In_2O_3 lattices without forming Mn metal and Mn-related oxide secondary phases. For the $(In_{1-x}Mn_x)_2O_3$ films with x = 0.085, 0.137, the peaks of the first Mn-O shell shift to higher R value (1.54 and 1.58 Å), indicating that the Mn-O bond length increases with Mn doping. In order to determine the accurate location of Mn atoms for all the $(In_{1-x}Mn_x)_2O_3$ films, we quantitatively fitted the experimental FT curves of the $(In_{1-x}Mn_x)_2O_3$ (x = 0.04, 0.05, 0.085, and 0.137) films, as shown in the dashed lines of Fig. 3. Some structure models have been applied during fitting process: ① structure model for Mn_{In1}; ② structure model for Mn_{In2}; ③ structure model for Mn metal; ④ structure model for MnO; ⑤ structure model for Mn_2O_3. We attempted to fit the FT curves for the $(In_{1-x}Mn_x)_2O_3$ films by a two-phase fitting using model ① or ② and model ④ or ⑤, but failed (not shown here). It is found that the best fit to FT curves can be obtained by only using the model ①, not the model ②③④⑤, indicating that the doped Mn atoms substitute for the In_1 sites of In_2O_3 lattice. The fitting results reveal that within experimental error,

the coordination number and the Mn-O bond length in the $(In_{1-x}Mn_x)_2O_3$ films with x = 0.04 and 0.05 are about 4.8 ± 0.3, 2.03 ± 0.01 Å and 4.6 ± 0.3, 2.04 ± 0.01 Å, respectively. For pure In_2O_3, six oxygen ions are located around In ions. The decrease in the first-shell coordination number of Mn indicates the presence of oxygen vacancies in the films. With further increasing Mn concentration, the Mn-O bond length increases to 2.08 ± 0.01 Å and 2.11 ± 0.01 Å, respectively, for the $(In_{1-x}Mn_x)_2O_3$ films with x = 0.085 and 0.137. These results unambiguously confirm that the doped Mn ions occupy the In_1 sites of In_2O_3 lattices for all the films.

Figure 4 show the magnetic-field dependence of magnetization (M versus H) at 300 K for the $(In_{1-x}Mn_x)_2O_3$ (x = 0.04, 0.05, 0.085, and 0.137) films after the subtraction of the diamagnetic contribution from the substrate. For all the films at 300 K, the magnetization saturates at high magnetic fields and exhibits a clear hysteresis behavior at lower fields [the inset (a) of Fig. 4]. These features indicate the existence of robust RT ferromagnetism. The inset (b) of Fig. 4 shows the saturation magnetization (M_s) versus the Mn concentration in the $(In_{1-x}Mn_x)_2O_3$ films. One can see that the M_s does not vary monotonically with the increase of Mn concentration. The M_s increases dramatically with a maximum value as the Mn concentration increases from x = 0.04 to x = 0.05, and then decreases with further increasing Mn concentration. The nonmonotonic Mn concentration dependence of M_s is different from the previously reported cases of Mo-doped In_2O_3 and Fe-doped In_2O_3,[16,23] where the M_s decreases or increases monotonously with the increase of TM concentration. To check the effect of oxygen vacancy, the argon flow rate is fixed at 10 sccm, and the oxygen flow rate is varied from 0 to
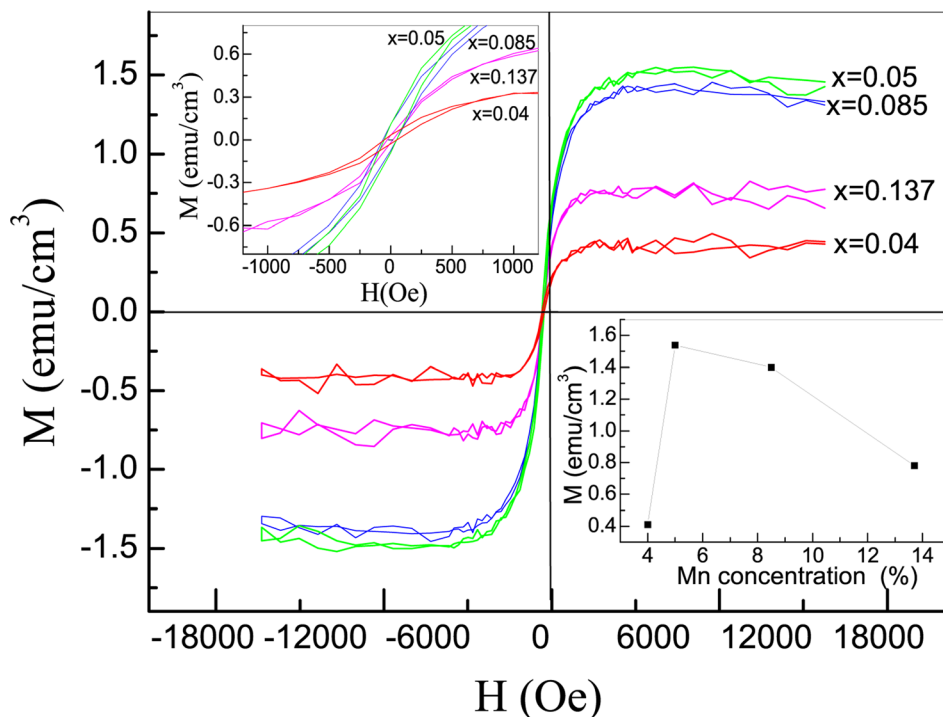

FIG. 4. (Color online) Hysteresis loops at 300 K of the $(In_{1-x}Mn_x)_2O_3$ (x = 0.04, 0.05, 0.085, and 0.137) films. Inset (a) shows the enlarged M-H curves at low magnetic field. Inset (b) shows the saturation magnetization (M_s) vs the Mn concentration.
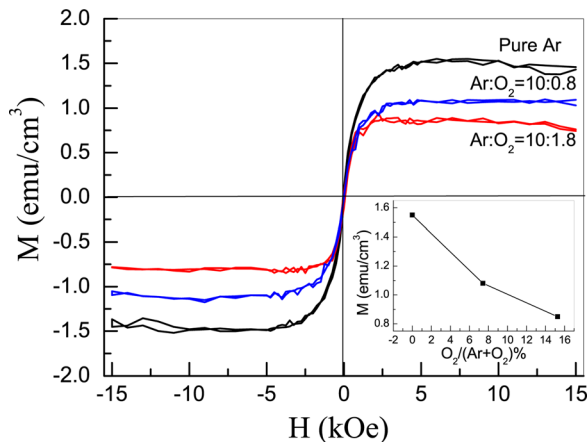
FIG. 5. (Color online) Hysteresis loops at 300 K of the $(In_{0.95}Mn_{0.05})_2O_3$ films deposited at oxygen flow rate of 0, 0.8, and 1.8 sccm.
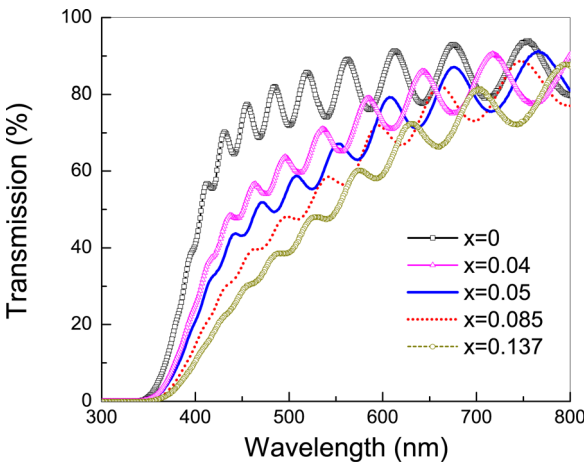

FIG. 6. (Color online) UV-vis transmission spectra of the $(In_{1-x}Mn_x)_2O_3$ (x = 0, 0.04, 0.05, 0.085, and 0.137) films.

1.8 sccm during the deposition. According to the EDS results, the nonstoichiometric formula for the $(In_{0.95}Mn_{0.05})_2O_3$ films deposited at oxygen flow rate of 0, 0.6, and 1.5 sccm were determined to be $(In_{0.95}Mn_{0.05})_2O_{2.47}$, $(In_{0.95}Mn_{0.05})_2O_{2.67}$, and $(In_{0.95}Mn_{0.05})_2O_{2.82}$, indicating that the concentration of oxygen vacancy decreases with the increase of the oxygen flow rate. Figure 5 show hysteresis loops of the $(In_{0.95}Mn_{0.05})_2O_3$ films deposited at oxygen flow rate of 0, 0.8, and 1.8 sccm. It is obvious that the M_s decreases from 1.54 to 0.84 emu/cm^3 with the increase of oxygen flow rate. These indicated that the oxygen vacancies should play an important role on the ferromagnetism.

The carrier concentration and resistivity were measured at room temperature by Hall measurements. These results are summarized in Table I. The type of carriers is confirmed to be n-type for all the $(In_{1-x}Mn_x)_2O_3$ films, as expected for films growth in an oxygen-deficient environment. The carrier concentration and resistivity in the $(In_{0.96}Mn_{0.04})_2O_3$ film is 3.3×10^{18} cm^{-3} and 5.1×10^{-2} $(\Omega \cdot cm)$, respectively. With further increasing Mn concentration, the carrier concentration n_c decreases and resistivity ρ increases monotonically in the films. It may be due to that the electrons arising from the oxygen vacancies may be partly compensated by the holes produced by the substitution of Mn^{2+} for In^{3+}, resulting in decreasing the carrier concentration n_c, and then the scattering from more Mn^{2+} ions may also contribute to the increase in the resistivity.

Figure 6 shows the UV-vis transmission spectra of the $(In_{1-x}Mn_x)_2O_3$ (x = 0, 0.04, 0.05, 0.085, and 0.137) films. For the optical measurement, the films were deposited on

ultrawhite glass substrates. The transmission spectra of the films show waveforms (ripples), which is the characteristic of the interference of light. All the films have about 70–80% of transmittance within the visible light and a large portion of the UV region is absorbed. The transmittance intensity of the films slightly decreases with the increase of Mn concentration. The optical bandgap E_g can be determined by measuring absorption coefficient (α) given by the following equation:[24] $\alpha = \ln(1/T)/d$, where T is transmittance and d is the film thickness. The optical bandgap dependence of the absorption coefficient (α) is given by the following equation: $(\alpha h \nu) = A(h\nu - Eg)^{1/2}$, where A and Eg are constant and optical bandgap, respectively. The optical bandgap can be calculated by plotting $(\alpha h \nu)^2$ versus $h\nu$ and extrapolating the linear portion of the plot to $(\alpha h \nu)^2 = 0$, as shown in Fig. 7. The error for optical bandgap values is about 0.01 eV. The inset of Fig. 7 shows the variation of optical bandgap values as a function of Mn concentration. The optical bandgap decreases (red-shift) with the increase of Mn concentration, which is consistent with the variation of Mn-O bond distance. According to the EXAFS results, the Mn-O bond distance increases with Mn doping; this can lead to weaken the

TABLE I. Summary of the carrier concentration, resistivity, and optical bandgap data for the $(In_{1-x}Mn_x)_2O_3$ (x = 0.04, 0.05, 0.085, and 0.137) films measured at 300 K. n_c denotes the carrier concentration, ρ the resistivity, and E_g the optical bandgap.

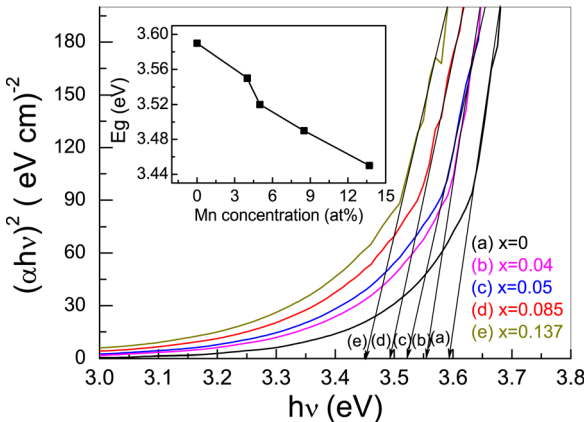| $(In_{1-x}Mn_x)_2O_3$	n_c (10^{18} cm^{-3})	ρ (10^{-2} $\Omega \cdot$cm)	E_g (eV)
x = 0	5.0	0.42	3.59
x = 0.04	3.3	5.1	3.55
x = 0.05	2.3	48	3.52
x = 0.085	1.8	102.6	3.49
x = 0.137	1.1	163.6	3.45

FIG. 7. (Color online) Dependence of $(\alpha h \nu)^2$ on photon energy ($h\nu$) for the $(In_{1-x}Mn_x)_2O_3$ (x = 0, 0.04, 0.05, 0.085, and 0.137) films at 300 K. The inset shows the variation of optical bandgap values as a function of Mn concentration.

interaction between Mn and O atoms, and further decrease the optical bandgap. Some reports in the literature have also observed the red-shift in the bandgap energy as the TM doped concentration is increased.[25,26] The red-shift can be attributed to the sp-d exchange between the In_2O_3 band electrons and localized d-electrons associated with the doped Mn cations. The exchange interaction leads to corrections in the energy bands, namely, the conduction band is lowered and the valence band is raised causing the bandgap to shrink.[27] Figure 8 shows the variation of optical bandgap E_g with respect to $n_c^{2/3}$, where n_c is the carrier concentration. The linear functional dependence is consistent with Burstein–Moss shift arguments in the context of nearly free electron model under the Fermi statistics for a degenerate n-type semiconductor.[28,29] However, one can see that there still exist some deviations from linearity between E_g and $n_c^{2/3}$, as shown in the inset of Fig. 8. It maybe due to that there exist dual conduction paths, resulting from the dual-band scenario. This two-band model could properly reconcile the deviation from linearity, but still need further investigation. The systematic change of optical bandgap with the increase of Mn concentration suggests the Mn atoms substitution for In ions in the lattice of In_2O_3 that causes the carrier concentration to change. These further verify that the room-temperature ferromagnetism in the $(In_{1-x}Mn_x)_2O_3$ films comes from Mn substitution.

The origin of ferromagnetism in TM-doped In_2O_3 has been very controversial due to the reported presence of mental cluster and/or metal-related secondary magnetic phase. The detailed structure analyses by XRD, XANES, and EXAFS strongly suggest that Mn ions substitute for the In^{3+} sites of In_2O_3 lattice and have ruled out the possibility of Mn-related secondary phases or clusters as the source of RT ferromagnetism. If the observed ferromagnetism origins from these n-type charge carriers, it can be expected that the M_s has the same decrease tendency with Mn doping. However, the M_s increased first and then decreases. So, it can be concluded that the observed RT ferromagnetism in the $(In_{1-x}Mn_x)_2O_3$ films does not result from the carrier-mediated exchange interaction. Recently, Coey *et al.* proposed bound magnetic polarons (BMP) mechanism

involving oxygen vacancies (V_O), which form F-centers with trapped electrons. Overlap of the F-center electron orbitals with the d orbitals of the neighboring TM spins to form TM-V_O-TM groups is crucial for the observed ferromagnetism.[30] When the concentration of oxygen vacancies is low, only isolated BMPs are expected in the lattice, and no long range ferromagnetism occurs. Only with the oxygen vacancies concentration increasing above a certain percolation threshold, these BMPs would overlap with each other, giving rise to long range ferromagnetism. So, BMP interactions involving oxygen vacancies can be account for the ferromagnetic order in the $(In_{1-x}Mn_x)_2O_3$ films. However, further experimental and the theoretical investigations are needed to address this issue and are now in progress.

IV. CONCLUSIONS

In summary, we have deposited the RT ferromagnetic $(In_{1-x}Mn_x)_2O_3$ films by RF-magnetron sputtering technique. Structural, optical, and magnetic properties of the $(In_{1-x}Mn_x)_2O_3$ films were studied systematically with respect to Mn concentration by XRD, UV-vis, XAS, and magnetic measurements. All the $(In_{1-x}Mn_x)_2O_3$ films display a clear RT ferromagnetism behavior. The observed ferromagnetism is of intrinsic origin, arising from the substitution of Mn for In sites of the In_2O_3 lattice and does not arise from Mn-related secondary phases or clusters in the films. The optical bandgap of films decreases monotonically with the increase of Mn concentration, which is agreement with the variation of carrier concentration in the films. The M_s of films increases first and then decreases with the increase of Mn concentration. It can be concluded that the oxygen vacancies play a mediation role on the ferromagnetic couplings between the Mn ions, and the BMP mechanism can be account for the ferromagnetic order in the $(In_{1-x}Mn_x)_2O_3$ films.
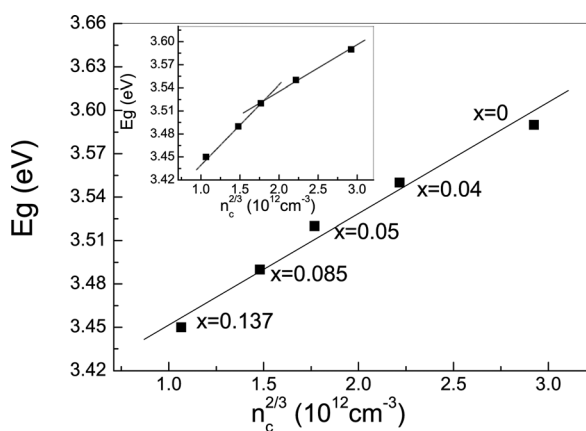
FIG. 8. Variation of optical bandgap E_g with respect to $n_c^{2/3}$. The inset shows the deviations from linearity between E_g and $n_c^{2/3}$.

[1]H. Ohno, Science **281**, 951 (1998).
[2]K. Asano, S. Doi, H. Yamaguchi, T. Komiyama, Y. Chonan, and T. Aoyama, J. Vac. Sci. Technol. A **29**, 03A119 (2011).
[3]B. Zhang, Q. H. Li, L. Q. Shi, H. S. Cheng, and J. Z. Wang, J. Vac. Sci. Technol. A **26**, 1469 (2008).
[4]C. B. Fitzgerald, M. Venkatesan, A. P. Douvalis, S. Huber, J. M. D. Coey, and T. Bakas, J. Appl. Phys. **95**, 7390 (2004).
[5]Y. B. Jiang, W. B. Mi, E. Y. Jiang, and H. L. Bai, J. Vac. Sci. Technol. A **27**, 1172 (2009).
[6]S. Q. Wang, Y. K. An, D. Q. Feng, Z. H. Wu, and J. W. Liu, J. Appl. Phys. **113**, 153901 (2013).
[7]J. Philip, N. Theodoropoulou, G. Berera, J. S. Moodera, and B. Satpati, Appl. Phys. Lett. **85**, 777 (2004).
[8]X. Q. Meng, L. M. Tang, and J. B. Li, J. Phys. Chem. C **114**, 17569 (2010).
[9]A. M. H. R. Hakimi, M. G. Blamire, S. M. Heald, M. S. Alshammari, M. S. Alqahtani, D. S. Score, H. J. Blythe, A. M. Fox, and G. A. Gehring, Phys. Rev. B **84**, 085201 (2011).
[10]H. Kim, M. Osofsky, M. M. Miller, S. B. Qadri, R. C. Y. Auyeung, and A. Pique, Appl. Phys. Lett. **100**, 032404 (2012).

[11] F. X. Jiang *et al.*, J. Appl. Phys. **109**, 053907 (2011).

[12] C. Y. Hsu, J. Phys. D: Appl. Phys. **44**, 415303 (2011).

[13] P. Kharel, C. Sudakar, M. B. Sahana, G. Lawes, R. Suryanarayanan, R. Naik, and V. M. Naik, J. Appl. Phys. **101**, 09H117 (2007).

[14] R. R. Ma, F. X. Jiang, X. F. Qin, and X. H. Xu, Mater. Chem. Phys. **132**, 796 (2012).

[15] N. H. Hong, J. Sakai, N. T. Huong, and V. Brize, J. Magn. Magn. Mater. **302**, 228 (2006).

[16] C. Y. Park, S. G. Yoon, Y. H. Jo, and S. C. Shin, Appl. Phys. Lett. **95**, 122502 (2009).

[17] C. Y. Park, C. Y. You, K. R. Jeon, and S. C. Shin, Appl. Phys. Lett. **100**, 222409 (2012).

[18] F. X. Jiang, X. H. Xu, J. Zhang, X. C. Fan, H. S. Wu, and G. A. Gehring, Appl. Phys. Lett. **96**, 052503 (2010).

[19] S. C. Li, P. Ren, B. C. Zhao, B. Xia, and L. Wang, Appl. Phys. Lett. **95**, 102101 (2009).

[20] A. P. S. Gaur, S. Sahoo, R. K. Katiyar, C. Rinaldi, J. F. Scott, and R. S. Katiyar, J. Phys. D: Appl. Phys. **44**, 495002 (2011).

[21] G. Peleckis, X. L. Wang, and S. X. Dou, J. Magn. Magn. Mater. **301**, 308 (2006).

[22] M. F. Bekheet, M. R. Schwarz, M. M. Muller, S. Lauterbach, H. J. Kleebe, R. Riedel, and A. Gurlo, RSC Adv. **3**, 5357 (2013).

[23] X. H. Xu, F. X. Jiang, J. Zhang, X. C. Fan, H. S. Wu, and G. A. Gehring, Appl. Phys. Lett. **94**, 212510 (2009).

[24] T. Asanuma, T. Matsutani, C. Liu, T. Mihara, and M. Kiuchi, J. Appl. Phys. **95**, 6011 (2004).

[25] S. V. Bhat and F. L. Deepak, Solid State Commun. **135**, 345 (2005).

[26] X. Liu, E. Shi, Z. Chen, H. Zhang, L. Song, H. Wang, and S. Yao, J. Cryst. Growth **296**, 135 (2006).

[27] X. L. Wang, C. Y. Luan, Q. Shao, A. Pruna, C. W. Leung, R. Lortz, J. A. Zapien, and A. Ruotolo, Appl. Phys. Lett. **102**, 102112 (2013).

[28] O. Lozano *et al.*, Sol. Energy Mater. Sol. Cells **113**, 171 (2013).

[29] S. M. Park, T. Ikegami, K. Ebihara, and P. K. Shin, Appl. Surf. Sci. **253**, 1522 (2006).

[30] J. M. D. Coey, M. Venkatesan, and C. B. Fitzgerald, Nat. Mater. **4**, 173 (2005).